JOURNAL OF PROPULSION AND POWER
Vol. 27, No. 3, May–June 2011

Erosion in Solid-Propellant Rocket Motor Nozzles with Unsteady Nonuniform Inlet Conditions

Ju Zhang* and Thomas L. Jackson†
University of Illinois at Urbana–Champaign, Urbana, Illinois 61801
John Buckmaster‡
Buckmaster Research, Urbana, Illinois 61801
and
Fady Najjar§
Lawrence Livermore National Laboratory, Livermore, California 94550

DOI: 10.2514/1.47158

A computational framework is developed to investigate nozzle erosion in solid-propellant rocket motors. The calculations have several novel features. Among these is an accounting of three-dimensional effects, most strikingly for a vectored nozzle but also in the description of the turbulent flow. Also, instead of the hitherto universal strategy of merely solving the nozzle flow with uniform inlet conditions, strategies by which the chamber flow with its nonuniform efflux can be coupled to the nozzle flow while still resolving the nozzle boundary layer are discussed. The chamber flow is approximated by either full motor simulations, which do not resolve the boundary layer, or by an asymptotic strategy valid for slender chambers: one first used in turbulent boundary-layer studies. The manner in which the chamber efflux conditions are used as nozzle inlet conditions is part of the discussion. The results suggest that specifying turbulent rather than uniform inlet conditions can have a significant effect on nozzle erosion.

I. Introduction

CARBON–CARBON/GRAPHITE nozzles are often used in solid rocket motors (SRMs), because of their ability to retain their structural integrity under extreme thermal environments and the ease with which they can be machined to achieve a desired geometry. However, when exposed to hot oxidizing chemical species such as H_2O, OH, CO_2, O, and O_2, surface erosion can occur. During a long burn, this can be sufficient to alter the geometry (including the throat area) to an extent sufficient to alter the rocket performance. For this reason, there is a need for theoretical and numerical studies that can lead to an understanding of the major factors that dictate the erosion rate and can lead to design improvements. Such studies present serious challenges, for not only must the chamber flow be well described to determine the nozzle inlet conditions (itself a challenging problem), but the nozzle flow must be well described, with full resolution of the boundary layers. Limitations to model complexity imposed by limited computer resources are an unavoidable constraint on any study.

Early work goes back to the 1960s [1,2]. Later, more comprehensive studies include work by Kuo and Keswani [3], further developed some 20 years later by Acharya and Kuo [4], and recent work by Thakre and Yang [5]. The last two publications provide the most significant discussions of the problem. They focus on erosion at the throat, where the consequences are most important because of the attendant throat area change. They argue that mechanical erosion for metalized propellants is unimportant, and the fundamental erosive mechanism is chemical reaction between the solid carbon surface and gaseous H_2O, OH, and CO. Both adopt the same global reaction mechanisms and parameters, but Acharya and Kuo [4] also examine a significant modification of the OH reaction. Thus, the only role that aluminum plays is its impact on the equilibrium chemical composition of the gases entering the nozzle. Acharya and Kuo [4] neglect gas-phase reactions; Thakre and Yang [5] include the water-shift reaction but conclude that it is unimportant, having no significant effect on either the concentrations of the oxidizing species or on the temperature.

Two interesting limits can be discussed, controlled by the surface temperature. When the latter is high, the heterogeneous reaction rates are fast, and the reaction is diffusion controlled. When it is low, so that the rates are slow, the reaction is rate controlled. Both limits can be well approximated, depending on the nature of the propellant. The diffusion limit is of particular interest insofar as validation is concerned, because with the uncertainties of mechanical erosion and reaction rates eliminated, the problem is merely one of mechanics and, with a suitable turbulence model, accurate predictions might be hoped for. Indeed, Thakre and Yang [5] are able to make very favorable comparisons with measurements of a ballistic test and evaluation system (BATES) motor for aluminized propellants at different metal loadings at a pressure of 6.9 MPa. Comparisons are also made with two other sets of rocket data, with good agreement even when the kinetics play an important role. It is noted that for pressures above 10 MPa, the OH concentrations are so small that the OH reaction can be neglected.

Acharya and Kuo [4] identify a much more important role for OH, even though the equilibrium values at low pressures (0.008 and 0.006 for their two propellants) are comparable to the value 0.01 identified by Thakre and Yang [5]. Significant OH effects are identified for pressures up to 55 MPa by comparison of erosion rates calculated using the modified or unmodified kinetics. Indeed, it is presumably these differences that were the motivation for the modification. Only one validation test is presented (modified kinetics). It is hard to evaluate the agreement for the nonaluminized propellant, because of the way the results are presented and because of what appears to be a significant error band for the experimental data. For the aluminized propellant, agreement is poor: the calculated rate being 50% larger than the experimental rate.

Presented as Paper 2009-5499 at the 45th AIAA/ASME/SAE/ASEE Joint Propulsion Conference and Exhibit, Denver, CO, 5–8 August 2009; received 16 September 2009; revision received 31 December 2010; accepted for publication 31 December 2010. Copyright © 2011 by the authors. Published by the American Institute of Aeronautics and Astronautics, Inc., with permission. Copies of this paper may be made for personal or internal use, on condition that the copier pay the $10.00 per-copy fee to the Copyright Clearance Center, Inc., 222 Rosewood Drive, Danvers, MA 01923; include the code 0748-4658/11 and $10.00 in correspondence with the CCC.

*Research Scientist, Computational Science and Engineering; juzhang@illinois.edu. Senior Member AIAA (Corresponding Author).
†Senior Research Scientist, Computational Science and Engineering; tlj@illinois.edu. Associate Fellow AIAA.
‡Proprietor.
§Code Physicist; najjar2@llnl.gov. Senior Member AIAA.

Returning to Thakre and Yang [5], there are three assumptions worthy of discussion: the inlet flow to the nozzle is assumed to be uniform so that turbulent fluctuations and fluctuations arising from combustion of the heterogeneous propellant are neglected, the heterogeneous reaction rates used were validated for subatmospheric pressures [6] and yet are assumed valid for the high pressures (4 MPa or higher) that prevail at the nozzle throat, and the wall thermal layer is assumed to be one-dimensional (and the wall normal is approximated by the nozzle radius vector). The latter is a poor approximation for the convergent section of the BATES nozzle, where the wall angle is approximately 45 deg. Thus, the success of the validation is unexpected, although it is possible that the poor modeling of the BATES nozzle is unimportant in the diffusion limit.

The assumption of uniform inlet flow is current industry practice, even when the flow of aluminum oxide particles is accounted for. Not only is the distribution of these across the inlet not uniform, but they also have a size distribution. Calculations that reveal these distributions are reported in [7,8] and the tools used in these calculations are available to us, but the computational costs force us to omit them. However, we do examine the effects of nonuniform flows, the essential focus of our study. Note that it has often been argued that mechanical erosion because of particle impact is negligible at the throat, because impact is negligible there, and the latter claim is supported by the calculations of [7]. It is a different matter if one is interested in erosion in the converging section of the nozzle or throat erosion in a vectored nozzle.

Another omission in [4,5] is an accounting of three-dimensional effects, whether in turbulence or geometry; axisymmetric flow is assumed. We abandon that restriction and examine both three-dimensional turbulence and vectored (nonaxisymmetric) nozzles.

Ideally, our simulations would include full motor (chamber plus nozzle) simulations, but this we cannot do while, at the same time, resolving the nozzle boundary layer. And so, we split the problem, solving the chamber flow and then using the efflux conditions from the chamber as inlet conditions for a fully resolved nozzle calculation. The patching between the two flows is an essential ingredient, one previously discussed for a jet flow [9]. At our call are two strategies for calculating the chamber flow: a full motor simulation sans resolution of the nozzle boundary layer and an asymptotic description (albeit numerical) valid for high-aspect-ratio chambers.

The fundamental numerical tool that we have at our disposal, always used when the asymptotic strategy is not being used (and therefore always used in the nozzle), is Rocstar, an inhouse code [10–13]. It is fully three-dimensional and is a tightly coupled fluid-structure-thermal multiphysics solver.

Movement of the nozzle surface, unsteady gas/solid coupling, and unsteadiness in the thermal field of the solid are all, quite reasonably, neglected. Also, we neglect gas-phase chemical reactions, noting that only insignificant effects are reported in [5]. The effects of oxidizers in the gas that play an important role in the erosion (recall the opening remarks in Sec. I) are modeled using a standard pyrolysis law dependent on the surface temperature and pressure, thus bypassing uncertainties in the surface reaction rates. Also, as noted earlier, aluminum particles are not included. By no means do we carry out a definitive study but focus rather on the difference between results for uniform nozzle inflow and results for nonuniform inflow.

The structure of the paper is as follows. Section II gives the mathematical formulation. In particular, the governing equations for the gas flow in the nozzle and for heat conduction in the nozzle walls are given, along with a methodology for gas–solid phase coupling. The asymptotic formulation for the chamber flow is also described. Section III discusses the numerical strategies for solving the equations of Sec. II, together with a description of the patching between the chamber flow and the nozzle flow. Section IV presents several verification tests. Section V presents results for the BATES motor, and erosion rates are calculated for both a straight nozzle and a rotated (gimbaled) nozzle. Concluding remarks appear in Sec. VI.

II. Mathematical Formulation

A. Gas Phase

The three-dimensional equations in the gas phase consist of Favre-averaged mass, momentum, and energy conservation for a viscous, compressible, ideal gas and are written as

$$\partial_t \bar{\rho} + \partial_j(\bar{\rho}\tilde{u}_j) = 0 \tag{1}$$

$$\partial_t(\bar{\rho}\tilde{u}_i) + \partial_j(\bar{\rho}\tilde{u}_i\tilde{u}_j) + \partial_i\bar{p} - \partial_j\tilde{\sigma}_{ij} = -\partial_j(\bar{\rho}\tau_{ij}) \tag{2}$$

$$\partial_t(\bar{\rho}\tilde{E}) + \partial_j[(\bar{\rho}\tilde{E} + \bar{p})\tilde{u}_j] - \partial_j(\tilde{\sigma}_{ij}\tilde{u}_i - \tilde{q}_j) = -\alpha_1 - \alpha_2 - \alpha_3 + \alpha_4 \tag{3}$$

where Reynolds averaging is denoted by an overbar and Favre averaging is denoted by a tilde. The viscous stress terms and heat flux terms are $\tilde{\sigma}_{ij}$ and $\tilde{q}_j$, expressed in terms of averaged variables, $\tilde{E}$ is the specific total energy,

$$\tilde{E} = \tilde{h} - \frac{\bar{p}}{\bar{\rho}} + \frac{\tilde{u}_j\tilde{u}_j}{2} \tag{4}$$

and $\bar{\rho}\tau_{ij}$ is the Reynolds stress,

$$\bar{\rho}\tau_{ij} = \overline{\rho u_i'' u_j''} \tag{5}$$

where $(\cdot)''$ terms are perturbations from the Favre mean. The turbulence terms in Eq. (3) are given by

$$\alpha_1 = \tilde{u}_i\partial_j(\bar{\rho}\tau_{ij}) \tag{6}$$

$$\alpha_2 = \partial_j(\overline{p'u_j''})/(\gamma - 1) \tag{7}$$

$$\alpha_3 = \overline{p'\partial_j u_j''} \tag{8}$$

$$\alpha_4 = \overline{\sigma_{ij}\partial_j u_i''} \tag{9}$$

where $(\cdot)'$ terms are perturbations from the Reynolds mean.

A variety of turbulence models, including Reynolds-averaged Navier–Stokes (RANS), large-eddy simulation (LES), and detached-eddy simulation (DES) are available in the computational framework and provide a closure model for the Reynolds stresses as well as the $\{\alpha_i\}$ [14,15]. LES, however, is computationally expensive for high-Reynolds-number flows due to the extremely fine mesh requirement near wall regions. Thus, in the results shown in this paper, the DES model is used [14]. DES is a simple modification of the Spalart–Allmaras (SA) turbulent model and switches from RANS(SA) to LES-like away from solid surfaces. This saves computational cost by increasing the resolution in the wall-normal direction while keeping the resolution in other directions relatively coarse. It is especially suitable for resolving the nozzle boundary layer.

B. Multiscale (Asymptotic) Formulation

Rocflo (Sec. III.A) is necessarily used in computing the nozzle flow, but its use for the chamber in the two-step strategy is expensive, and so, for exploratory work, we use a simpler strategy. This is rooted in an asymptotic analysis for which direct numerical simulations (DNSs) can be performed for the turbulent chamber flow. It was first devised and used by Spalart for turbulent boundary layers [16], by Venugopal et al. [17] for planar SRMs, and by Isfahani et al. [18] to examine the effect of turbulence on propellant flames.

Within the SRM context, it determines the flow dynamics at any plane with streamwise location $x/h = 1/\epsilon$, where ϵ is a small parameter, x is the distance from the head end, and h is the half-width (radius) of the chamber for a planar (cylindrical) geometry. Asymptotic analysis valid in the limit of vanishing ϵ (which, as in all asymptotic analyses, we hope is accurate for small but finite values of physical interest) removes the overall axial gradients and generates a problem with periodic boundary conditions at the upstream and

downstream ends in which the gradient effects appear as source terms in the evolution equations [17]. The geometric parameter is ϵ, but it is also the ratio of the mass injection rate to the mean flow rate [17] at location x/h.

Our formulation here is restricted to incompressible flow, valid only for rocket chambers of modest size. The chambers are either planar or cylindrical, but the turbulent field for the cylindrical geometry can be three-dimensional. Although temperature fluctuations could be generated at the propellant surface, we do not account for them. Then, the governing equations are

$$\nabla \cdot \mathbf{V} = S_\rho \tag{10}$$

$$\frac{\mathrm{D}\mathbf{V}}{\mathrm{D}t} + \nabla p - \frac{1}{Re}\nabla \cdot \tau_{ij} = \mathbf{S}_\mathbf{v} \tag{11}$$

Here, $Re = V_{\text{inj}}h/\nu$ is the Reynolds number based on the injection velocity V_{inj} and the chamber half-width (radius) h for a planar (cylindrical) geometry. The source terms S_ρ and $\mathbf{S}_\mathbf{v}$ arise as part of the multiscale analysis [17] and are given by

$$S_\rho = -\epsilon u_x \tag{12}$$

$$S_{u_x} = -\epsilon u_x^2 + \pi^2/\epsilon \tag{13}$$

$$S_{u_r} = -\epsilon u_x u_r' \tag{14}$$

$$S_{u_\theta} = -\epsilon u_x u_\theta' \tag{15}$$

for cylindrical geometry [19].

C. Solid Phase

The solid phase is usually modeled as a homogeneous material. Then, a one-dimensional heat equation is solved in the direction normal to the nozzle surface, a strategy justified when the thermal-layer thickness is small compared with the nozzle radius; typical values for operational rockets are 1 cm and 1 m, respectively.

In a frame attached to the nozzle surface, we have

$$c_c\left(\rho_c \frac{\partial T_c}{\partial t} + M\frac{\partial T_c}{\partial n}\right) = \frac{\partial}{\partial n}\left(\lambda_c \frac{\partial T_c}{\partial n}\right) \tag{16}$$

subject to the boundary conditions

$$\left.\frac{\partial T_c}{\partial n}\right|_{\text{surface}} = g \tag{17}$$

$$\left.\frac{\partial T_c}{\partial n}\right|_{(n\to-\infty)} = 0 \tag{18}$$

Here, T_c is the temperature, λ_c is the thermal conductivity, ρ_c is the density, c_c is the specific heat, $M = \rho_c \dot{r}_c$ is the mass flux with $\dot{r}_c$ the erosion rate, and n is the distance along the wall normal. The term g is related to conditions in the gas phase, discussed in the next subsection. A variation on this formulation, one used by Acharya and Kuo [4] and Thakre and Yang [5], assumes that the normal distance can be well approximated by the radial distance. This is clearly reasonable where the slope of the nozzle wall is small (close to the throat) and in the divergent section. But in the BATES nozzle, a commonly used testbed that we discuss later, the slope of the convergent section can be as large as 45 deg.

D. Gas–Solid Phase Coupling

The nozzle surface is an interface between the condensed phase and the gas phase, and certain connection conditions are imposed there, in addition to a formulation for the erosion rate. Thus, the tangential velocities are equal, as are the normal mass fluxes in a surface-fixed frame:

$$\tilde{u}_t = 0 \tag{19}$$

$$\bar{\rho}_g(\tilde{u}_n + \dot{r}_c) = \rho_c \dot{r}_c \tag{20}$$

Energy conservation has the form

$$[c]M\tilde{T}_s = \lambda_g \mathbf{n}\cdot\nabla\tilde{T}_g - \lambda_c \mathbf{n}\cdot\nabla T_c - MQ_s \tag{21}$$

where $[\cdot] \equiv (\cdot)_g - (\cdot)_c$, and Q_s is the surface heat release, with a characteristic value of 125 kJ/mol (or 10.4 kJ/g for carbon) defined by thermodynamics [3] by the reaction

$$\mathrm{C}_{(s)} + \mathrm{H_2O} \rightarrow \mathrm{CO} + \mathrm{H_2} \tag{22}$$

The convention here is that Q_s is positive when the reaction is endothermic and negative when exothermic. The temperature is continuous, $[T] = 0$.

The connection conditions are essentially those of [5]. Even so, we knowingly neglect terms related to turbulent fluctuations. For example, Eq. (20) would assume the following form:

$$\bar{\rho}_g(\tilde{u}_n + \dot{r}_c) + \overline{\rho_g' u_n''} = \rho_c \dot{r}_c \tag{23}$$

if terms related to turbulent fluctuations were accounted for. However, to keep such terms would require closure modeling, but we neither know how to model them, nor do we have the tools to perform a DNS to develop appropriate subgrid models.

The erosion rate is determined from a pyrolysis law,

$$\dot{r}_c = A_c \bar{p}^\beta \exp\left(\frac{-E_c}{R_u \tilde{T}_s}\right) \tag{24}$$

where E_c is the activation energy, R_u is the universal gas constant, and $\tilde{T}_s$ is the surface temperature. Representative values are $\beta = 0.5$ and $E_c/R_u = 34,625$ K for the reaction shown in Eq. (22) [6]. The empirical parameter A_c is chosen such that a desired erosion rate is reached under certain operating conditions, determined from experiments or more detailed numerical simulations. Thus, our predictions are comparative only and not absolute. We comment here that the particular form of the pyrolysis law [Eq. (24)] neglects temperature fluctuations in the Arrhenius term.

At steady state, Eq. (16) can be integrated, and the solution is substituted into Eq. (17) to give

$$\left.\frac{\partial T_c}{\partial n}\right|_{\text{surface}} = g_o = (\dot{r}_c/\alpha_c)(\tilde{T}_s - T_{-\infty}) \tag{25}$$

where g_o is the steady-state value of g, $\dot{r}_c$ is given by Eq. (24), and α_c is the thermal diffusivity in the solid phase. Substituting this equation into the energy balance equation (21), we obtain

$$\begin{aligned}\lambda_g \left.\frac{\partial \tilde{T}}{\partial n}\right|_g &= \lambda_c g_o + MQ_s + [c]M\tilde{T}_s \\ &= \lambda_c(\dot{r}_c/\alpha_c)(\tilde{T}_s - T_{-\infty}) + MQ_s + [c]M\tilde{T}_s\end{aligned} \tag{26}$$

This equation relates the surface temperature to the gas-phase surface heat flux at steady state. The equations in the gas phase are now closed with the boundary conditions defined by Eqs. (19), (20), and (26).

We use the steady-state description in our calculations and neglect geometry changes due to surface regression. Rocflo can accommodate both effects, if necessary, but implementation would be expensive.

III. Numerical Strategies

A. Rocflo

The gas-phase Eqs. (1–3), subject to the boundary conditions in Eqs. (19), (20), and (26), are solved using Rocflo [13], with DES for the turbulence model [14]. The equations are discretized in time using an explicit four-step Runge–Kutta method. A second-order

finite volume central scheme is used for spatial discretization. Specifically, the scheme is based on cell-centered control volumes for the convective terms. The code includes provision for artificial dissipation, but this is not used in the present simulations. Convective fluxes through the control volume faces are approximated using averaged variables.

The viscous terms are discretized in a similar fashion, making use of an auxiliary control volume shifted by a half grid cell in each computational direction. The auxiliary control volumes are used for the first derivatives, and the primary ones (grid cells) are used for the second derivatives.

We use Rocflo for all of the nozzle calculations and for some full-rocket simulations.

B. Asymptotic Strategy

Equations (10) and (11) are not turbulence equations in the usual sense of that rubric, and so which numerical strategies might work well or not for turbulence equations is not a relevant matter. In fact, a suitable tool is the high-order incompressible scheme described in [20]. Thus, the convective terms are discretized using the fifth-order weighted essentially nonoscillatory (WENO) scheme of [21], making it possible to resolve difficult applications with strong shear or turbulence. Also, the fractional-step scheme of [22] together with the optimized two-step alternating 4–6 low-dissipation and low-dispersion Runge–Kutta scheme of [23] is used to improve temporal accuracy.

C. Patching the Chamber and Nozzle Solutions

Our two-step strategy first requires the calculation of the chamber flow, using either the asymptotic strategy or a coarse-mesh full motor simulation. Once initial transients have disappeared, flow data are extracted at a plane upstream of or at the nozzle inlet for a suitable time interval. An upstream choice is necessary when using the asymptotic strategy, as it is inaccurate at points within a chamber diameter or so of the nozzle; the time interval must be long enough for the subsequent calculation of the nozzle flow.

The extraction is done uniformly in time, and the data are linearly interpolated for the fine-mesh nozzle simulations in both time and space. Rocflo uses the stagnation pressure, stagnation temperature, and the direction of the velocity vector at the upstream boundary. Overall, a database is created of inlet conditions at discrete times and places for a time period equal to the total time for which the nozzle integration is carried out.

IV. Preliminary Calculations and Verification

A. Solution of Asymptotic Equations

We refer to [19] for detailed discussion and more results on the solution of the asymptotic equations. Here, the results of a test calculation are shown for a cylindrical chamber and three-dimensional turbulence. The injection velocity is one, $Re = 1000$, and $\epsilon = 0.04$ (i.e., $x/R = 25$).

The circumferential vorticity is shown in Fig. 1. The small-scale structures that we expect to find in a turbulent flow are apparent, and we note that evidence that the asymptotic strategy generates authentic turbulent flows is presented in [17,19].

Some general remarks can be made about the nature of the turbulence. Velocities are nondimensionalized using the injection speed (typically 2.5–3.2 m/s) for a wide range of rocket sizes. Also, the maximum nondimensional rms of u_x for $\epsilon = 0.04$ and $Re \sim 1000$–5000 is ~ 10 at $r \sim 0.98$; for a longer chamber with $\epsilon = 0.025$; this maximum increases to ~ 15, again with little variation with Re. Thus, the magnitude of the dimensional velocity fluctuations for our simulation is characteristic of a wide range of rocket sizes. However, the reference frequency is V_{inj}/h, so that the dimensional frequency changes significantly with rocket size.

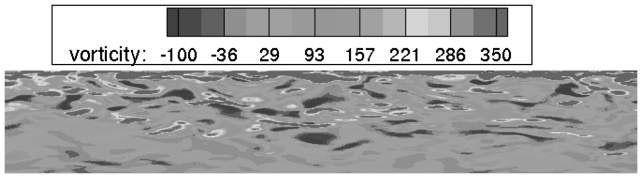

Fig. 1 Circumferential vorticity ω_θ field in a three-dimensional cylindrical multiscale simulation with an Re of 1000 and ϵ of 0.04. The top wall at $r = 1$ is the injecting boundary. The mesh is 128^3.

B. Compressible Laminar Boundary Layer

Hitherto, Rocflo has not been used for simulations in which a heat flux boundary condition is used, and so we verify that ingredient by examining a boundary-layer configuration for which there are well-known theoretical results (a similarity solution) rooted in the Illingworth transformation [24]. This boundary layer sits on a flat plate (no slip and no injection) with a surface temperature gradient

$$\frac{\partial T}{\partial y} = T_e \sqrt{\frac{U_e}{2\nu_e x}} g'$$

where $T_e = 288$ K, $U_e = 170$ m/s, $\nu_e = 0.034$ m/s^2, and $g' = 0.01$. The freestream Mach number is 0.5, the Prandtl number is equal to one, and the viscosity is proportional to T. The distance from the leading edge x is equal to 0.5 m when $Re = 2500$. Figure 2 shows the temperature profiles calculated using Rocflo and calculated via the similarity solution.

C. Solution Patching

We examine the 70 lb BATES motor (also known as BATES70) described by Geisler et al. [25]. A schematic is shown in Fig. 3; details of the geometry and other relevant parameters can be found in [7]. It should be noted that the propellant charge is exposed at the nozzle end so that there is no reason to expect a toroidal eddy in the acute angle between the propellant and the nozzle.

In the absence of imposed perturbations of significant amplitude, the flow is laminar [7] in both planar and axisymmetric geometries. We consider the planar one and impose a periodic injection (burning) rate in order to test our strategy within an unsteady context. Thus,

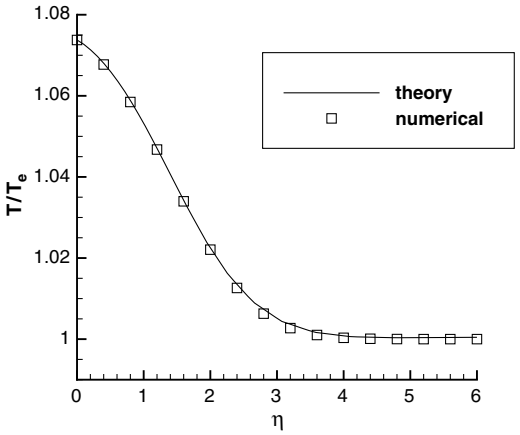

Fig. 2 Profiles of temperature (normalized by the freestream temperature) at $x = 0.5$ m for a laminar boundary layer over a flat plate, with heat transfer at a Mach number of 0.5; $\eta = \sqrt{\frac{U_e}{2\rho_e \mu_e x}} \int_0^y \rho \, dy$.

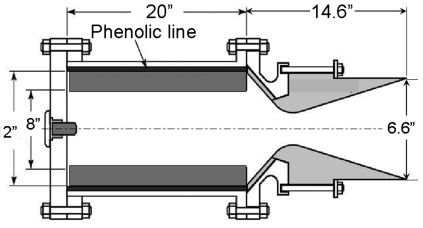

Fig. 3 Schematic of BATES configuration.

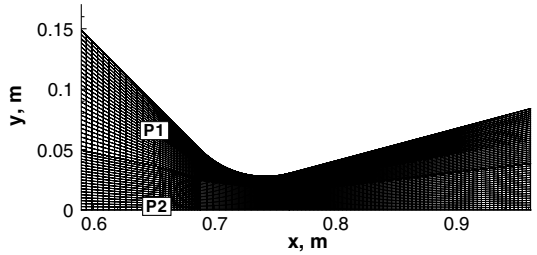

Fig. 4 Positions of the stations for the histories shown in the verification study. P1 and P2 are (0.65,0.068) and (0.65,0) m. Mesh for simulations where the boundary layer is unresolved is also shown.

$$\dot{m} = \dot{m}_o(1 + 0.1\sin(\omega t)) \tag{27}$$

where $\dot{m}_o = 25.7$ kg/m^2-s and $\omega = 2000$ Hz. The nozzle wall is treated as a no-slip adiabatic surface.

The full motor configuration includes a chamber of length 0.51 m and a height of 0.1 m. Within this chamber, a uniform 40×35 mesh is used. The coarse mesh in the nozzle is 105×49; see Fig. 4.

For the nozzle-only calculation, an additional 36 mesh points are added in y within a layer of thickness 0.85 mm, which contains the boundary layer. Although 105 mesh points are still used in x, some stretching is applied with a spacing of approximately 0.5 mm near the inlet, and a spacing of approximately 2 mm is applied well downstream.

Comparisons between the densities at two different stations calculated in the two different ways are shown in Fig. 5. Note that the nozzle boundary layer in the full-configuration simulation is unresolved, whereas it is resolved in the nozzle-only simulations. Both simulations are viscous.

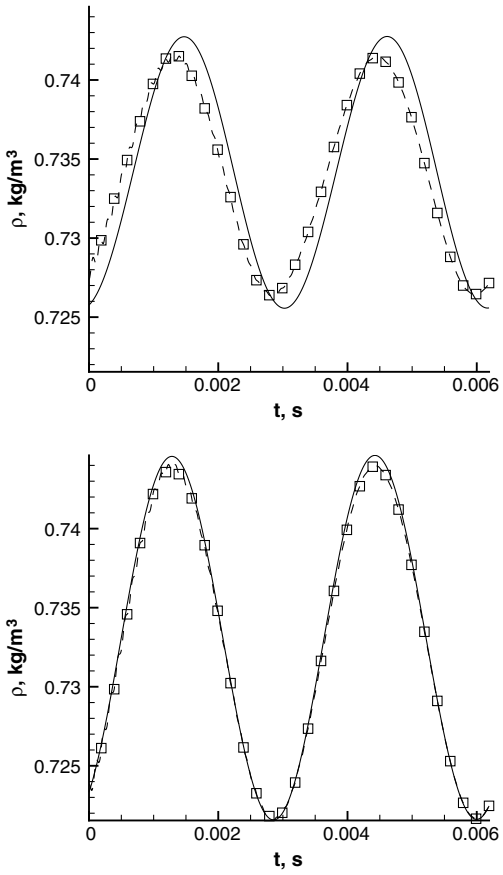

Fig. 5 Comparison of density evolution of full-configuration (solid) and nozzle-only (symbols) planar BATES70 simulations at quasi steady states for P1 (top) and P2 (bottom), shown in Fig. 4. The differences are of order 0.1–0.2%. Similar agreements are observed for other stations examined, not shown here.

V. Erosion in Ballistic Test and Evaluation System Nozzles

In this section, we describe a number of flow simulations using the BATES nozzle, for different inlet conditions, and with a focus on nozzle erosion. In one simulation, we generate three-dimensional effects by tilting the nozzle. We noted earlier that, for operational rockets, the thermal layer in the solid is thin compared with the nozzle radius, and so it is essentially planar. This is only a rough approximation for laboratory rockets, such as the BATES, but it is acceptable since our results have only a comparative value.

A. Grid Issues

We start with a brief examination of errors that can arise from grid choices: specifically, the grid size and the cell aspect ratio. The tests are for the planar nozzle only, with uniform inlet conditions.

Consider Fig. 6. This shows an example of the evolution of the mesh in the normal direction in the vicinity of a small surface patch, with 36 points along the normal within 0.85 mm of the surface. Figure 7 shows the temperature profile and the heat flux profile along the normal at $x = 0.692$ m for four meshes characterized by 24, 48, 96, and 192 points within the 0.85 mm layer. Note that, for this particular x location, there are $\sim 0.5n$ grid points inside the boundary layer, where n (identified in the figures) is the number of grid points in the wall-normal direction inside a 0.85 mm layer at the nozzle surface. Also, in Fig. 8, the erosion rates along the surface are shown for these resolutions. (The kink at $x \approx 0.69$ m occurs at the transition between the conical inlet and the curvilinear throat section.) Convergence is first order near the surface, and it is second order as the interior is approached. Note that the erosion rates are unphysically small for these planar simulations, as the parameters used are relevant to the three-dimensional simulations that we describe in the next section.

The aspect ratio of the mesh cells can be varied by varying the grid spacing in the x direction. When varied in this way for the smallest cells, no significant solution effects are found.

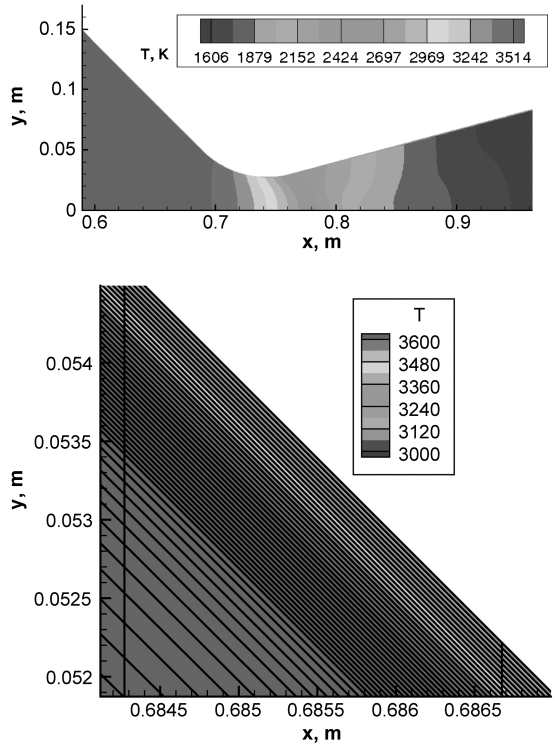

Fig. 6 Temperature field of a planar BATES70 nozzle with uniform inlet condition ($P_o = 2$ MPa, $T_o = 3650$ K) and 36 grid points in the wall layer of 0.85 mm thick along the surface. The bottom graph shows the close-up view in the boundary layer. The mesh used is also plotted.

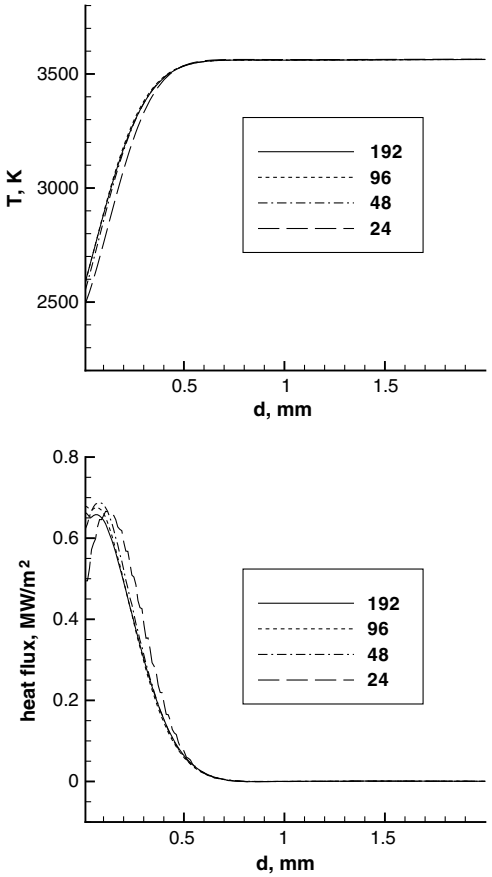

Fig. 7 Profiles of temperature (top) and heat flux (bottom) at $x = 0.692$ m near the throat along the wall-normal direction for the planar case. The relative differences in temperature and heat flux, i.e., $|(s_{192} - s_{96})/s_{192}|$. with s being either temperature or heat flux, at the wall are 0.1 and 2.4%, respectively, between the solutions by resolutions 96 and 192, indicating convergence.

B. Three-Dimensional (Nonaxisymmetric) Effects

Three-dimensional effects arise in the nozzle as the result of the nature of the turbulent flow, nonuniform inlet conditions, or a nontrivial geometry that leads to three-dimensional flows even when the nozzle geometry itself is axisymmetric. For example, for the ONERA-86 rocket [14], the flow at the nozzle inlet is turbulent. It is worth noting that significant three-dimensional temperature fluctuations downstream can also arise merely because a heterogeneous propellant is used [26]. Thus, Fig. 9 shows the temperature

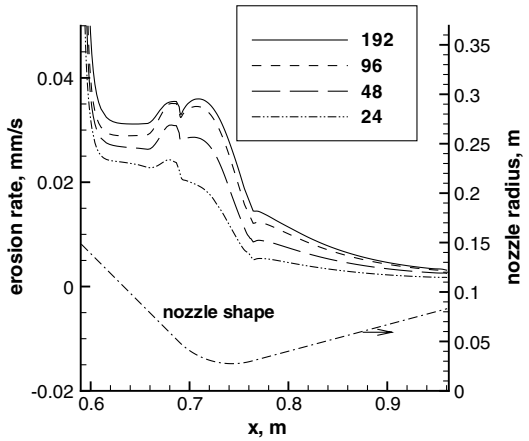

Fig. 8 Erosion rate along the nozzle surface at different resolutions. The numbers identify the number of grid points in the wall-normal direction inside a 0.85 mm layer at the nozzle surface.

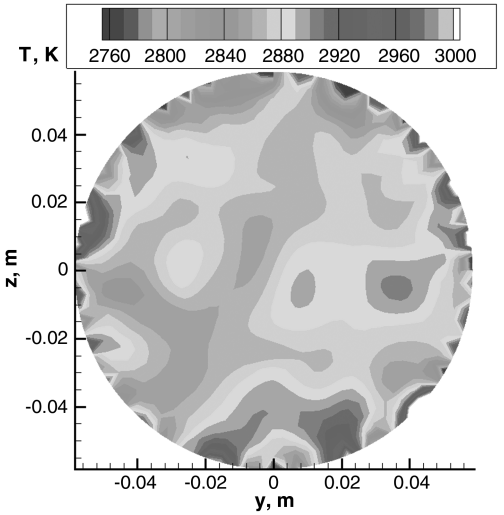

Fig. 9 Temperature field at the nozzle inlet extracted from a full-configuration BATES15 simulation.

field at the nozzle inlet generated by a full-configuration (chamber and nozzle) BATES15 simulation; the flow is assumed to be laminar. Also, the multiscale rocket simulation results shown in Fig. 1 reveal turbulence sufficiently far downstream.

Our purpose is to see if fluctuations in the chamber can have an effect on nozzle erosion and so should be accounted for. One way to do this is to extract the flowfield at the inlet plane in a full-configuration three-dimensional turbulent simulation, and then use

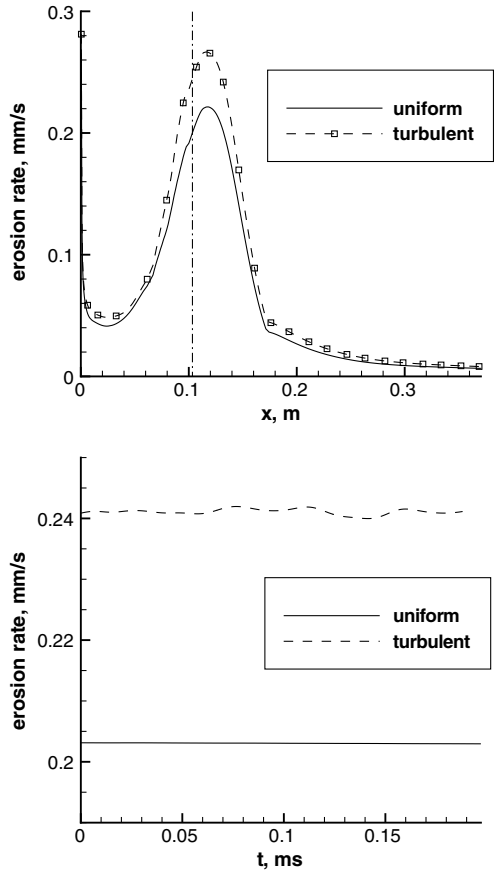

Fig. 10 Erosion rates along the nozzle surface for simulations of a straight BATES nozzle using either turbulent or uniform inlet conditions (top). The difference near the throat can be as large as 20%. The x axis is the distance from the nozzle inlet plane. Time history of the erosion rate near the throat at $x \sim 0.1$ m, marked by the dashed–dotted line in the top graph (bottom). DES is used for both simulations with $C_{\mathrm{DES}} = 0.65$.

those data in a fine-resolution nozzle-only simulation, as discussed in Sec. I. An alternative approach, as we have already noted, is to calculate the inlet conditions using the multiscale strategy. For example, the data obtained in the multiscale rocket simulation discussed in Sec. III.B can be used as the turbulent inlet condition for a three-dimensional BATES70 nozzle simulation. This we do, and proper reference scales based on the physical parameters of the BATES motor are used to obtain dimensional values. In particular, the time histories of the velocity components are collected at the inlet plane at uniform time intervals. The patching method discussed in Sec. III.C and verified in Sec. IV is then used for velocities at the inlet plane in the subsequent Rocflo nozzle-only simulation. The temperature is simply perturbed and periodic in time:

$$T = T_o[1 + 0.1\sin(2\pi f t)] \tag{28}$$

where $T_o = 3650$ K and $f = 2000$ Hz. We specify the temperature independently of the velocity because we are solving the incompressible multiscale equations in the chamber. In the future, we hope to develop a high-order code to solve the compressible multiscale equations. In addition to imposing unsteady inlet conditions, we also examine three-dimensional effects induced by a nontrivial geometry by considering a gimbaled or thrust vector control nozzle. The configuration is generated by rotating the axisymmetric BATES nozzle 25 deg about the z axis while retaining a small portion of the unrotated chamber.

1. *Straight Nozzle*

We first examine a straight (axisymmetric) nozzle and compare the axial distribution of the erosion rate for uniform and nonuniform inlet conditions. Results are shown in Fig. 10, with the most significant difference occurring near the throat. Note that the overall magnitude of these rates is consistent with empirical data [25], but only because A_c in the pyrolysis law equation (24) was judiciously chosen. We are a long way from first-principle absolute predictions. Note that the relatively high erosion rate at $x = 0$ is an artifice of the BATES configuration where the propellant charge is exposed at the nozzle end (see the discussion of Fig. 3 in Sec. IV.C). Even though high erosion is generally not desired anywhere, rocket performance will be most affected by throat erosion. Temporal variations near the throat are shown in the bottom graph of Fig. 10 and reveal a roughly 20% increase because of nonuniform inflow. For a 100 s burn, this corresponds to nearly 5 mm more erosion.

2. *Gimbaled Nozzle*

Our three-dimensional code enables us to examine gimbaled nozzles, a problem that we do not believe has been previously addressed. The vorticity fields at some arbitrarily chosen time are shown in Fig. 11. Not surprisingly, the erosion rate at the bottom is greater than at the top, by significant amounts (Fig. 12). Note also that the differences due to nonuniform inlet conditions are greater for the bottom than for the top, the difference for the former being approximately 22% at the throat.

It might have been thought that tilting a nozzle would have a significantly deleterious effect on that part of the nozzle in the extrapolated path of the chamber efflux, but comparing Fig. 10 and 12, we see that throat erosion at the bottom for the tilted nozzle is not much greater than throat erosion for the straight nozzle. It is unlikely that this would be true for metalized propellants.

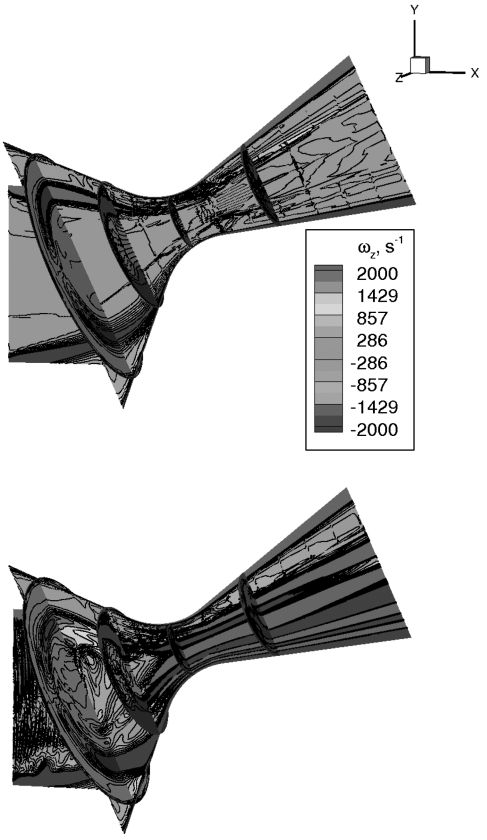

Fig. 11 Instantaneous z-vorticity fields in the gimbaled BATES nozzle with uniform (top) and turbulent (bottom) inlet conditions. For the uniform inlet conditions, $P_o = 6.5$ MPa and $T_o = 3650$ K. For the turbulent inlet conditions, the inlet temperature is given by Eq. (28), the velocities from the multiscale simulation, and pressure is determined from outgoing characteristics and oscillates around 6.5 MPa. The contour levels are adjusted to enhance the feature near the inlet.

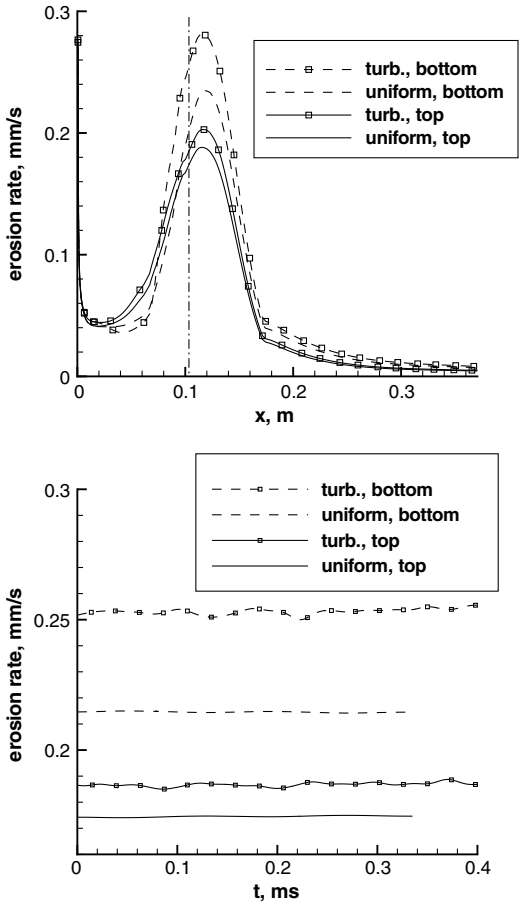

Fig. 12 Erosion rates along the top and bottom intersections of the $z = 0$ plane and the gimbaled BATES nozzle surface for simulations using either turbulent or uniform inlet conditions (top). Time history of the erosion rate near the throat of the gimbaled BATES nozzle (bottom). Both the top and bottom stations, marked by the dashed–dotted line in the top graph, are located at the same distance of ∼0.1 m from the nozzle inlet plane.

VI. Conclusions

In this paper, nozzle erosion has been investigated and three ingredients not present in previous studies have been included: three-dimensional (not axisymmetric) turbulence, turbulent inlet conditions at the nozzle, and gimbaling. It has been shown that the second ingredient can increase the throat erosion by about 20%, and that a nozzle that has acceptable erosion characteristics when straight can be tilted without incurring a significant loss of those characteristics for nonmetalized propellants.

The model does, of course, have several deficiencies/omissions, approximations, and modeling ingredients justified, which is believed due to the focus on whether or not inlet fluctuations should be accounted for. For gimbaled nozzles, the most important omission must surely be the role of metal particles; although there are good, albeit expensive, tools for describing particle transport [7], calculating the erosive effect of their impact is a challenging problem. For nongimbaled nozzles with a concern with only throat erosion, a proper accounting for surface chemistry is necessary when the oxidizer fluxes are not diffusion limited, and there are serious reservations as to the applicability of the data from [6] to the conditions prevailing in a rocket, despite the apparent success of the validation tests of Thakre and Yang [5]. One promising situation for which nonempirical science-based predictions might become routinely reliable is throat erosion in the diffusion limited regime. High accuracy might then be possible, provided fluctuations are fully accounted for. In this connection, it would be important to explore the variations in the erosion rate with the frequency of the inlet turbulence (see the remark at the end of Sec. IV.A).

Acknowledgments

This work was supported through Buckmaster Research, under grant FA9550-07-C-0123, under a Small Business Technology Transfer Phase II program with the U.S. Air Force, program manager A. Nachman. This work was partially supported by the U.S. Department of Energy through the University of California, under subcontract B523819, by NASA Constellation University Institutes Project, under grant NCC3-989, and through the University of Maryland, under subcontract Z634015, with Claudia Meyer as the project manager.

References

[1] Delaney, L. J., Eagleton, L. C., and Jones, W. H., "A Semiquantitative Prediction of the Erosion of Graphite Nozzle Inserts," *AIAA Journal*, Vol. 2, No. 8, 1964, pp. 1428–1433. doi:10.2514/3.2570

[2] McDonald, A. J., and Hedman, P. O., "Erosion of Graphite in Solid-Propellant Combustion Gases and Effects on Heat Transfer," *AIAA Journal*, Vol. 3, No. 7, 1965, pp. 1250–1257. doi:10.2514/3.3117

[3] Kuo, K. K., and Keswani, S. T., "A Comprehensive Theoretical Model for Carbon-Carbon Composite Nozzle Recession," *Combustion Science and Technology*, Vol. 42, Nos. 3–4, 1985, pp. 145–164. doi:10.1080/00102208508960374

[4] Acharya, R., and Kuo, K. K., "Effect of Chamber Pressure and Propellant Composition on Erosion Rate of Graphite Rocket Nozzle," *Journal of Propulsion and Power*, Vol. 23, No. 6, 2007, pp. 1242–1254. doi:10.2514/1.24011

[5] Thakre, P., and Yang, V., "Chemical Erosion of Carbon-Carbon/Graphite Nozzles in Solid-Propellant Rocket Motors," *Journal of Propulsion and Power*, Vol. 24, No. 4, 2008, pp. 822–833. doi:10.2514/1.34946

[6] Bradley, D., Dixon-Lewis, G., Habik, El-Din, S., and Mushi, E. M., "The Oxidation of Graphite Powder in Flame Reaction Zones," *20th Symposium (International) on Combustion*, Combustion Inst., Pittsburgh, PA, 1984, pp. 931–940.

[7] Haselbacher, A., and Najjar, F. M., "Multiphase Flow Simulations of Solid-Propellant Rocket Motors on Unstructured Grids," 44th AIAA Aerospace Sciences Meeting and Exhibit, AIAA Paper 2006-1292, Jan. 2006.

[8] Najjar, F. M., Ferry, J., Haselbacher, A., and Balachandar, S., "Simulations of Solid-Propellant Rockets: Effects of Aluminum Droplet Size Distribution," *Journal of Spacecraft and Rockets*, Vol. 43, No. 6, 2006, pp. 1258–1270. doi:10.2514/1.17326

[9] Glaze, D. J., and Frankel, S. H., "Stochastic Inlet Conditions for Large-Eddy Simulation of a Fully Turbulent Jet," *AIAA Journal*, Vol. 41, No. 6, 2003, pp. 1064–1073. doi:10.2514/2.2073

[10] Dick, W., Heath, T., Fiedler, R., and Brandyberry, M., "Advanced Simulation for Solid Propellant Rockets," 41st AIAA/ASME/SAE/ASEE Joint Propulsion Conference and Exhibit, AIAA Paper 2005-3990, 2005.

[11] Jiao, X., Zheng, G., Lawlor, O. S., Alexander, P. J., Campbell, M. T., Heath, M. T., and Fiedler, R. A., "An Integration Framework for Simulations of Solid Rocket Motors," 41st AIAA/ASME/SAE/ASEE Joint Propulsion Conference and Exhibit, AIAA Paper 2005-3991, 2005.

[12] Massa, L., Jackson, T. L., and Buckmaster, J., "Using Heterogeneous Propellant Burning Simulations as Subgrid Components of Rocket Simulations," *AIAA Journal*, Vol. 42, No. 9, 2004, pp. 1889–1900. doi:10.2514/1.4445

[13] Blazek, J., "Flow Simulation in Solid Rocket Motors Using Advanced CFD," AIAA/ASME/SAE/ASEE Joint Propulsion Conference and Exhibit, AIAA Paper 2003-5111, 2003.

[14] Wasistho, B., and Moser, R. D., "Simulation Strategy of Turbulent Internal Flow in Solid Rocket Motor," *Journal of Propulsion and Power*, Vol. 21, No. 2, 2005, pp. 251–263. doi:10.2514/1.7760

[15] Wasistho, B., Balachandar, S., and Moser, R. D., "Compressible Wall-Injection Flows in Laminar, Transitional, and Turbulent Regimes: Numerical Prediction," *Journal of Spacecraft and Rockets*, Vol. 41, No. 6, 2004, pp. 915–924. doi:10.2514/1.2019

[16] Spalart, P., "Direct Simulation of a Turbulent Boundary Layer up to $Re_\theta = 1410$," *Journal of Fluid Mechanics*, Vol. 187, 1988, pp. 61–98. doi:10.1017/S0022112088000345

[17] Venugopal, P., Moser, R. D., and Najjar, F. M., "Direct Numerical Simulation of Turbulence in Injection Driven Plane Channel Flows," *Physics of Fluid*, Vol. 20, No. 10, 2008, Paper 105103. doi:10.1063/1.2963137

[18] Isfahani, A. H. G., Zhang, J., and Jackson, T. L., "The Effects of Turbulence-Induced Time-Periodic Shear on a Flame Anchored to a Propellant," *Combustion and Flame*, Vol. 156, No. 5, 2009, pp. 1084–1098. doi:10.1016/j.combustflame.2008.12.009

[19] Zhang, J., and Jackson, T. L., "Direct Numerical Simulation of Turbulence in Injection Driven Three-Dimensional Cylindrical Flows," *Journal of Fluid Mechanics* [online], 2011. doi:10.1017/S0022112010005215

[20] Zhang, J., and Jackson, T. L., "A High-Order Incompressible Flow Solver with WENO," *Journal of Computational Physics*, Vol. 228, No. 7, 2009, pp. 2426–2442. doi:10.1016/j.jcp.2008.12.009

[21] Jiang, G. S., and Shu, C. W., "Efficient implementation of weighted ENO schemes," *Journal of Computational Physics*, Vol. 126, No. 1, 1996, pp. 202–228. doi:10.1006/jcph.1996.0130

[22] Kim, J., and Moin, P., "Application of a Fractional-Step Method to Incompressible Navier–Stokes Equations," *Journal of Computational Physics*, Vol. 59, No. 2, 1985, pp. 308–323. doi:10.1016/0021-9991(85)90148-2

[23] Hu, F. Q., Hussaini, M. Y., and Manthey, J. L., "Low-Dissipation and -Dispersion Runge–Kutta Schemes for Computational Acoustics," *Journal of Computational Physics*, Vol. 124, No. 1, 1996, pp. 177–191. doi:10.1006/jcph.1996.0052

[24] Illingworth, C. R., "Some Solutions of the Equations of Flow of a Viscous Compressible Fluid," *Proceedings of the Cambridge Philosophical Society (Mathematical and Physical Sciences)*, Vol. 46, No. 3, 1950, pp. 469–478. doi:10.1017/S0305004100025986

[25] Geisler, R. L., Beckman, C. W., and Kinkead, S. A., "The Relationship between Solid Propellant Formulation Variables and Motor Performance," 11th AIAA/SAE Propulsion Conference, AIAA Paper 1975-1199, 1975.

[26] Massa, L., Jackson, T. L., Buckmaster, J., and Najjar, F., "Fluctuations Above a Burning Heterogeneous Propellant," *Journal of Fluid Mechanics*, Vol. 581, 2007, pp. 1–32. doi:10.1017/S0022112007005927

J. Powers
Associate Editor